



Cite this: *Soft Matter*, 2022, 18, 1525

Received 12th November 2021,  
Accepted 20th January 2022

DOI: 10.1039/d1sm01613j

rsc.li/soft-matter-journal

## An anisotropic immerse precipitation process for the preparation of polymer membranes

Xuwen Qiu,<sup>ab</sup> Sheng Mao,<sup>a</sup> Jun Yin<sup>id</sup><sup>c</sup> and Yantao Yang<sup>id</sup><sup>\*a</sup>

We study the immerse precipitation process in a ternary polymer/solvent/non-solvent system by numerically solving the two-dimensional Cahn–Hilliard phase field equation. In particular, we introduce anisotropic mobility, namely the mobility of a polymer varies over different spatial directions, and focus on the porosity morphology of the obtained polymer membrane. Simulations reveal that as the anisotropy increases in the polymer mobility, the polymer pattern changes from nearly isotropic and random voids to strips parallel to the direction with smaller mobility. The influence of anisotropy quickly saturates. The anisotropic mobility model is also applied to a ternary system mimicking the preparation of a hollow fiber membrane, and shows strong effects on the membrane porosity pattern.

### 1 Introduction

A membrane is an interface between two adjacent phases acting as a selective barrier, regulating the transport of substances between the two compartments.<sup>1</sup> Polymer membranes can be used in fields such as reverse osmosis and gas separation due to their good selectivity.<sup>2</sup> Besides, polymer membranes also have excellent bio-compatibility. Membranes with different porous morphologies and surface structures can be used for hemodialysis,<sup>2</sup> bio-detection,<sup>3</sup> *in vivo* treatment,<sup>4</sup> artificial tissue and organ generation,<sup>5</sup> *etc.*

There are different ways to prepare polymer membranes, and immerse precipitation is a very important and popular method for preparing polymer membranes. In the process of immerse precipitation, a polymer solution containing a polymer(p) and a solvent(s) precipitates into a coagulation bath of a non-solvent(n), in which the polymer does not dissolve. Phase separation occurs as the solvent dissolves into the non-solvent bath, and porous membranes are formed. For the immerse precipitation process, the physical and chemical properties of the material, polymer concentration, and temperature cast a significant influence on the formation mechanism that would eventually determine the morphology and the structure of polymer membranes.<sup>6</sup>

Usually, a ternary phase diagram, shown in Fig. 1, is used for describing the process of immerse precipitation. Each point

inside the triangle represents a composite of the ternary mixture polymer solution. There are two characteristic lines, namely the binodal and spinodal lines, on the phase diagram. Inside the spinodal line is the region unstable to infinitesimal disturbance of concentration. Between the spinodal and binodal lines is the meta-stable region, where a finite disturbance is required to trigger demixing. And, outside the binodal line is the stable region. In the process of immerse precipitation, the homogeneous polymer solution first lies outside the binodal line. Then the polymer solution is immersed into a non-solvent coagulation bath. As the solvent and non-solvent components inter-diffuse into each other, the ternary composite gradually moves into the meta-stable region where liquid–liquid demixing takes place. The system can further move inside the spinodal line and separate into a polymer-rich phase and a polymer-lean phase. Finally, the polymer-rich phase becomes the membrane while the polymer-lean phase becomes the pore.

There were already numerous experimental studies of the polymer membrane formation.<sup>7–17</sup> These experimental studies

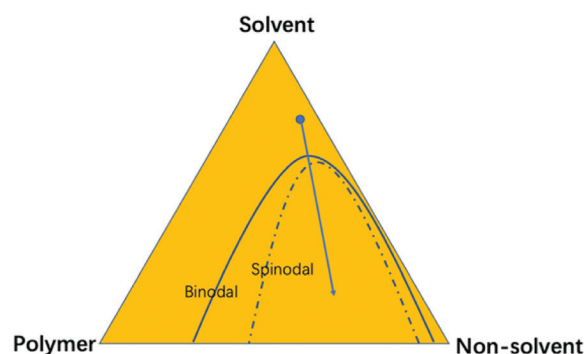


Fig. 1 Phase diagram of the polymer/solvent/non-solvent ternary system.

<sup>a</sup> State Key Laboratory for Turbulence and Complex Systems, Department of Mechanics and Engineering Science, College of Engineering, Peking University, Beijing 100871, China. E-mail: yantao.yang@pku.edu.cn

<sup>b</sup> Computational Engineering and Robotics Lab, Department of Mechanical Engineering, Carnegie Mellon University, Pittsburgh, PA, 15213, USA

<sup>c</sup> The State Key Laboratory of Fluid Power and Mechatronic Systems, School of Mechanical Engineering, Zhejiang University, Hangzhou, 310028, China

mainly focused on the concentration of the polymer solution, the flow rate of the dope fluid, the temperature, the effect of air gap in the spinning process and the effect of additives and obtained different types of structures, such as sponge-like layers and macrovoids. Theoretical and numerical studies have also been conducted to investigate the membrane formation process.<sup>18–23</sup> Various models and numerical methods were used for the problems, such as the multi-fluid model based on the Rayleigh function,<sup>20</sup> the Monte-Carlo simulation,<sup>24</sup> and the Lattice–Boltzmann method.<sup>25</sup>

Among all the models, the continuous Cahn–Hilliard model<sup>26</sup> is widely employed, not only for phase separation, but also for many other fields.<sup>27,28</sup> Zhou *et al.*<sup>18</sup> carried out simulations of the Cahn–Hilliard equation using the Flory–Huggins model. The results showed varying porous morphology with different initial compositions in 2D and 3D. They also found out that the hydrodynamic effect would destabilize the membrane interface. Manuel *et al.*<sup>19</sup> focused on the convection term of the Cahn–Hilliard equation, and introduced the velocity of a moving mixing interface as the velocity in the convective derivative. They obtained sponge pores, finger pores and lamella structures by adjusting the composite concentration and the velocity of the mixing interface.

The polymer membranes obtained in experiments can be very different in their porosity patterns, which depend on the material and the operating conditions. Anisotropy in porosity patterns can also be introduced intentionally by applying directional geometry confinement.<sup>29</sup> However, in most of the aforementioned studies, isotropic diffusivity or mobility was used. Anisotropic diffusion has been explored in several micro-scale simulations, such as the non-equilibrium molecular dynamics simulation<sup>30</sup> and the dynamical density functional theory.<sup>31</sup> In the current work, we employ the continuous model of Cahn–Hilliard equations, and investigate the effects of the anisotropic mobility at the macro-scale on the porosity patterns during the phase separation process. Considering that the polymer usually has a large molecule with a complex molecular configuration, it is plausible to assume that the polymer can diffuse with different speeds along different directions, especially when polymer molecules align along a specific direction.

The rest of the paper is organized as follows. In Section 2 we briefly describe the physical model, the governing equation, and the numerical details. Section 3 contains all the numerical results. Conclusions are given in Section 4.

## 2 Physical models and governing equations

Consider a ternary system consisting of three components, such as the polymer (p), solvent (s), and non-solvent (n). The volume fraction of each component is denoted by  $\phi$ . Due to the conservation of the total volume, one always has

$$\phi_p + \phi_s + \phi_n = 1, \quad (1)$$

and the system has only two independent unknowns, for which we choose  $\phi_p$  and  $\phi_s$ . Here we only briefly describe the key parts of the formulation. For complete details, the reader is referred to the original paper of Cahn and Hilliard.<sup>26</sup> We follow the notation of Zhou and Powell.<sup>18</sup> The diffusion of the component  $i$  (with  $i = p, s, \text{ or } n$ ) obeys the following equation:

$$\frac{\partial \phi_i}{\partial t} = \nabla \cdot \left( \sum_j M_{ij} \nabla \mu_j \right). \quad (2)$$

Here  $\mu_j$  is the chemical potential of the component  $j$ , and  $M_{ij}$  is the mobility associated with the diffusion of the component  $i$  caused by the gradient of the chemical potential of the component  $j$ , respectively. The mobility can depend on the local condition of the system. However, in the current study, we assume that they are spatially homogeneous.

For the chemical potential, we utilized the Flory–Huggins free energy model. The total free energy  $F$  is written as the volume integration of the free energy density

$$F = \int_V f(\mathbf{x}, \phi_i, \nabla \phi_i) dV. \quad (3)$$

The free energy density can be expressed as, for the ternary system,

$$f = f_0(\phi_p, \phi_s) + \frac{1}{2} [K_p (\nabla \phi_p)^2 + K_s (\nabla \phi_s)^2]. \quad (4)$$

Here  $K$  is the gradient penalty coefficient, and the cross gradient terms are neglected. The homogeneous part is given by the Flory–Huggins model as

$$f_0 = \frac{RT}{v_{\text{site}}} \left( \sum_{i=p,s,n} \frac{1}{m_i} \phi_i \ln \phi_i + \frac{1}{2} \sum_{i,j=p,s,n} \chi_{ij} \phi_i \phi_j \right). \quad (5)$$

Here  $R$  is the gas constant,  $T$  is the temperature,  $v_{\text{site}}$  is the volume per reference site,  $m$  is the degree of polymerization, and  $\chi_{ij}$  is the interaction parameters between the components  $i$  and  $j$ . For simplicity, we set  $m_s = m_n = 1$ .

The chemical potential  $\mu_i$  with  $i = s$  or  $p$  is then given by the functional variation derivatives of the total free energy  $F$  with respect to  $\phi_i$  as

$$\mu_i = \frac{\delta F}{\delta \phi_i} = \frac{\partial f_0}{\partial \phi_i} - K_i \nabla^2 \phi_i. \quad (6)$$

Substitute (6) into (2) and one gets

$$\frac{\partial \phi_p}{\partial t} = \nabla \cdot \left[ M_p \nabla \left( \frac{\partial f_0}{\partial \phi_p} - K_p \nabla^2 \phi_p \right) \right], \quad (7)$$

$$\frac{\partial \phi_s}{\partial t} = \nabla \cdot \left[ M_s \nabla \left( \frac{\partial f_0}{\partial \phi_s} - K_s \nabla^2 \phi_s \right) \right]. \quad (8)$$

Here we set  $M_{sp} = M_{ps} = 0$  and denote  $M_s = M_{ss}$  and  $M_p = M_{pp}$ , since the diffusion of one component caused by the gradient of the other component is minor in many cases.

Eqn (7) and (8) have been successfully used in the simulations of immerse precipitation,<sup>18</sup> where the porosity morphology of the membranes is spatially uniform within the initially

polymer-rich region. The variation of parameters, such as the mobility  $M$  and the initial composition of the ternary system, only change the typical size of the porous voids. As mentioned in the Introduction section, in the present work, we introduce anisotropy into the mobility parameter, specifically in that of the polymer component. That is, the mobility  $M_p$  takes different values for the diffusion along different directions. In the two-dimensional Cartesian coordinates, eqn (7) becomes

$$\frac{\partial \phi_p}{\partial t} = \left( M_{px} \frac{\partial^2}{\partial x^2} + M_{py} \frac{\partial^2}{\partial y^2} \right) \left( \frac{\partial f_0}{\partial \phi_p} - K_p \nabla^2 \phi_p \right), \quad (9)$$

where  $M_{px}$  and  $M_{py}$  have independent values. Since we will also simulate some cases in the two-dimensional cylindrical coordinates, we can write down the counterpart of eqn (9) as

$$\frac{\partial \phi_p}{\partial t} = \left[ \frac{M_{pr}}{r} \frac{\partial}{\partial r} \left( r \frac{\partial}{\partial r} \right) + \frac{M_{p\theta}}{r^2} \frac{\partial^2}{\partial \theta^2} \right] \left( \frac{\partial f_0}{\partial \phi_p} - K_p \nabla^2 \phi_p \right). \quad (10)$$

The Laplacian in cylindrical coordinates is

$$\nabla^2 = \frac{1}{r} \frac{\partial}{\partial r} \left( r \frac{\partial}{\partial r} \right) + \frac{1}{r^2} \frac{\partial^2}{\partial \theta^2}.$$

Anisotropy can also be introduced into the mobility of the solvent in the same way. Since the solvent usually has a much smaller molecule than the polymer, and in most cases the solvent component diffuses much faster than the polymer component, anisotropic solvent mobility only has minor effects on the morphology of the membrane porosity, which will be confirmed by our simulations as discussed in the next section. Moreover, it should be noted that in general,  $K$  is not a constant and usually depends on the concentration. Here, for simplicity and as done in many existing studies,  $K$  is kept constant in our simulations.

We numerically solve eqn (9) and (8) for the Cartesian box and (10) and (8) for the cylindrical domain. The centred finite difference scheme is used for the spatial discretization. For the time integration we use the same scheme as in refs. 32 and 33. Specifically, a Runge–Kutta type of scheme is utilized, with the fourth order terms treated semi-implicitly by the Crank–Nicolson method, and all the other terms explicitly by the Adams–Bashforth method. The time integration can self-start for each time step. We use the implicit scheme for the fourth order terms to reduce the constrain on the size of time step. The boundary condition is periodic or no-flux for both  $\phi$  and  $\mu$  depending on the exact setup of the problem, and will be specified during the discussion.

### 3 Results and discussion

In this section we present the simulation results of three different setups, and focus on how the anisotropic mobility affects the pattern morphology.

#### 3.1 Two-dimensional periodic box

The first case we simulate is the phase separation in a fully periodic two-dimensional box. Therefore, the periodic boundary condition is

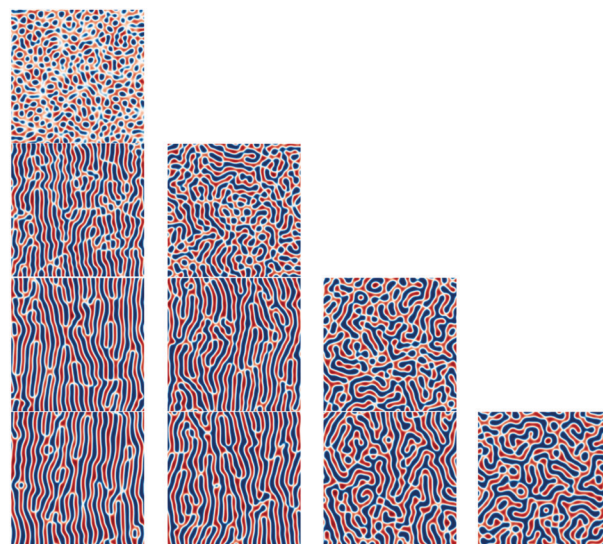


Fig. 2 Porosity morphology in periodic box simulations with different combinations of  $(M_{px}, M_{py})$  at the final stage. The red color represents the polymer-rich regions and the blue color represents the solvent-rich regions. The initial solution composite is  $(\phi_p, \phi_s) = (0.20, 0.20)$ . The rows from top to bottom have  $M_{px} = 1.0, 1.4, 1.8,$  and  $2.0$ , while the columns from left to right have  $M_{py} = 1.0, 1.4, 1.8,$  and  $2.0$ , respectively.

applied in both directions for all the quantities. We fix  $M_s = 2$ , and systematically change both  $M_{px}$  and  $M_{py}$  between 1.0 and 2.0. Coefficients  $\chi_{ij}$  are set as  $\chi_{ns} = 0.2$ ,  $\chi_{np} = 1$ ,  $\chi_{sp} = 0.3$ , and  $m_p = 64$ , respectively. The initial solution has  $\phi_p = 0.2$ ,  $\phi_s = 0.2$ , and  $\phi_n = 1 - \phi_p - \phi_s = 0.6$ . A white noise with a small magnitude is added to trigger the evolution. Due to the symmetry between the  $x$ - and  $y$ -directions, we also set  $M_{px} \geq M_{py}$  without losing generality. The domain has a unit length in both directions and the resolution is  $100 \times 100$ . Since we focus on the morphology of porosity patterns induced by the anisotropic mobility, we do not run our simulation until the coarsening stage, which requires much longer simulation times.

In Fig. 2 we compare the different patterns at the final stage of phase separation for different combinations of  $M_{px}$  and  $M_{py}$ . The panels are arranged in the matrix form according to the values of  $M_{px}$  and  $M_{py}$ . Therefore the diagonal panels exhibit isotropic mobility with different values, and the panels further away from the diagonal panels exhibit stronger anisotropy in the mobility. Clearly, as the anisotropy increases, the pattern shifts from a statistically homogeneous state to distinct strips with preferential directions. For the off-diagonal cases shown in Fig. 2,  $M_{px}$  is larger than  $M_{py}$  and the strips are along the vertical  $y$ -direction. That is, the diffusion in the horizontal  $x$ -direction is faster than that in the vertical direction, so that the phase separation is more pronounced in the  $x$ -direction. It should be pointed out that the initial perturbation is a white noise with a small amplitude which is statistically homogeneous in space; therefore the anisotropic pattern obtained here is the result of the anisotropic mobility coefficient.

To quantitatively analyze the anisotropy of the pattern after the phase separation, we first conduct the two-dimensional

Fourier transform of  $\phi_p$  for the cases shown in Fig. 2. The magnitude of the Fourier coefficients is shown in Fig. 3. For the diagonal panels with isotropic mobility, the contours of the Fourier coefficient magnitude are almost perfect circles, indicating that there is no preferential direction in the polymer pattern. For panels with large anisotropic mobility, indicating the off-diagonal panels, the contours have distinct peaks at a certain angle  $\psi$ , whose definition is illustrated in panel (a) of Fig. 3.

We then calculate the orientation order parameter  $S$  based on the Maier-Saupe distribution function. We follow the same procedure as used in refs. 29, 34 and 35. The contours of the Fourier coefficient magnitude shown in Fig. 3 are first integrated along the radial direction to obtain an intensity distribution over the azimuthal angle  $\psi$ . One of such azimuthal distribution is shown in Fig. 4 for the case with  $M_{px} = 1.8$  and  $M_{py} = 1.0$ . The two peaks locate at  $\psi \approx 90$  and  $270$ , indicating that the peak intensity in the Fourier coefficient magnitude is for the wavenumber vectors in the horizontal direction, and the corresponding structures orient vertically. The intensity curve is then fitted with the Maier-Saupe function

$$I = I_0 + A \exp[\alpha \cos^2(\psi - \psi_0)]. \quad (11)$$

Here  $I_0$  is the free base intensity,  $\alpha$  measures the width between the two peaks, and  $\psi_0$  is the azimuthal angle where the peaks locate. Once  $\alpha$  is obtained by fitting, the orientation order parameter can be computed by

$$S = \frac{\int_{-1}^1 P_2(\cos \beta) \exp[\alpha \cos^2 \beta] d(\cos \beta)}{\int_{-1}^1 \exp[\alpha \cos^2 \beta] d(\cos \beta)}, \quad (12)$$

where  $P_2(\cos \beta)$  is the Hermans orientation function

$$P_2(\cos \beta) = \frac{1}{2}(3 \cos^2 \beta - 1). \quad (13)$$

The orientation order parameter  $S$  can take values between 0 and 1. For a perfect isotropic pattern  $S = 0$ , and for a fully anisotropic pattern  $S = 1$ , respectively.

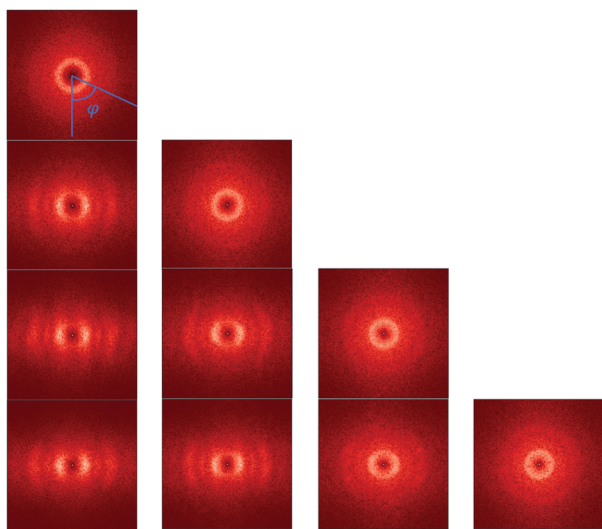


Fig. 3 Magnitude of the Fourier coefficients for the polymer distributions shown in Fig. 2. Panels have the same values for  $M_{px}$  and  $M_{py}$  as in Fig. 2.

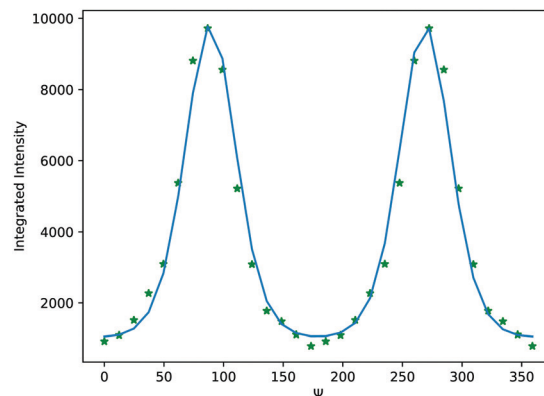


Fig. 4 Symbols are the intensity distribution given by the radial average of panel d in Fig. 3 with  $M_{px} = 1.8$  and  $M_{py} = 1.0$ . The curve is fitted with the Maier-Saupe function (11).

The orientation order parameter  $S$  is plotted against the ratio  $\Theta = M_{px}/M_{py}$  for different values of  $M_{py}$  in Fig. 5. For different values of  $M_{py}$ ,  $S$  exhibits similar dependence on  $\Theta$ . When  $\Theta$  is close to 1, indicating the isotropic mobility,  $S$  is around 0.2, which corresponds to a relatively isotropic pattern. As  $\Theta$  increases,  $S$  quickly increases with enhancing anisotropy in the polymer pattern. When  $\Theta > 2$ , the value of  $S$  saturates between 0.7 and 0.8. A further increment in  $\Theta$  has only minor effects on  $S$ . For  $\Theta$  at this range the pattern already becomes nearly parallel strips. It is also worthy pointing out that the ratio between  $M_{px}$  and  $M_{py}$  plays a central role in controlling the anisotropic pattern.

The anisotropic pattern produced by anisotropic mobility can be understood mathematically as follows. If one introduces the coordinate transformation as  $x' = x/\sqrt{\Theta}$ ,  $y' = y$ ,  $t' = M_{py}t$ , then eqn (9) can be cast into

$$\frac{\partial \phi_p}{\partial t'} = \left( \frac{\partial^2}{\partial x'^2} + \frac{\partial^2}{\partial y'^2} \right) \left( \frac{\partial f_0}{\partial \phi_p} - K_p \nabla^2 \phi_p \right). \quad (14)$$

Therefore, anisotropy with  $\Theta \neq 1$  can be regarded as a compression or expansion in the original  $x$ -direction and a related transformation

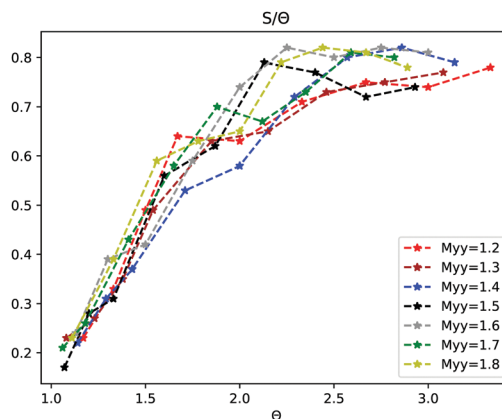


Fig. 5 The orientation order parameter  $S$  versus the mobility ratio  $\Theta$  for all the cases simulated.

of the time scale. In the new coordinate system  $x', y'$ , the pattern should be isotropic; then after transforming back to the coordinate system  $(x, y)$ , the isotropic pattern is stretched in the  $x$  direction and anisotropy emerges in the porosity pattern.

### 3.2 A specific ternary system case

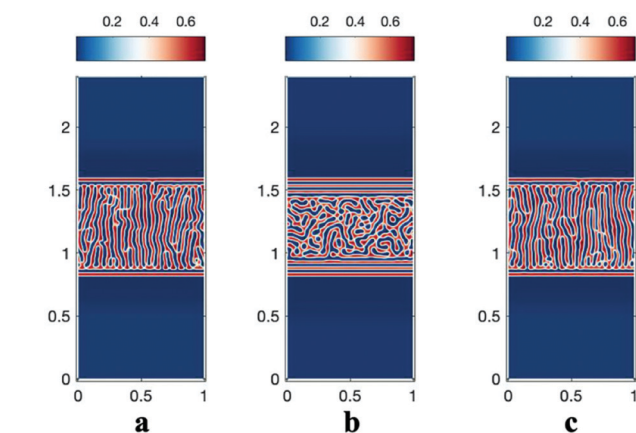
After showing that the anisotropic mobility can dramatically change the morphology of phase separation in the fully periodic box, we now turn to a specific water(n)/DMF(s)/PVDF(p) ternary system as studied by Zhou *et al.*<sup>18</sup> and introduce anisotropic mobility in this system. The simulation domain is set as those for the preparation of hollow fiber membranes (HFMs). In the horizontal  $x$ -direction, a periodic boundary condition is used. In the vertical  $y$ -direction, initially the polymer solution occupies the middle part with  $y_i \leq y \leq y_o$ , and the non-solvent coagulation bath locates at both sides. The impermeable boundary condition is used in the  $y$ -direction. The initial polymer solution composite has  $\phi_p = 0.3$  and  $\phi_s = 0.65$ . The solvent mobility is very different from the polymer mobility, for example, about 1000 times larger.  $m_p$  is reduced to 5 due to the large mobility coefficient used in this section. It should be pointed out that a precise measurement for the model coefficients in Cahn–Hilliard equations is very challenging, especially when one considers the anisotropy in mobility coefficients. For the current study we employ the empirical values used in previous studies.<sup>18</sup> A more systematic calibration of the coefficients in the current model against experiments is left for future studies.

In Fig. 6 we present the final pattern for different combinations of mobility. In particular, we also investigate the effects of anisotropic mobility for the solvent component. Three cases are simulated with either anisotropic solvent mobility, or anisotropic polymer mobility, or both. The results suggest that once the polymer component exhibits anisotropic mobility, *i.e.*  $M_{px} \neq M_{py}$ , the pattern changes to a strip shape. However, the

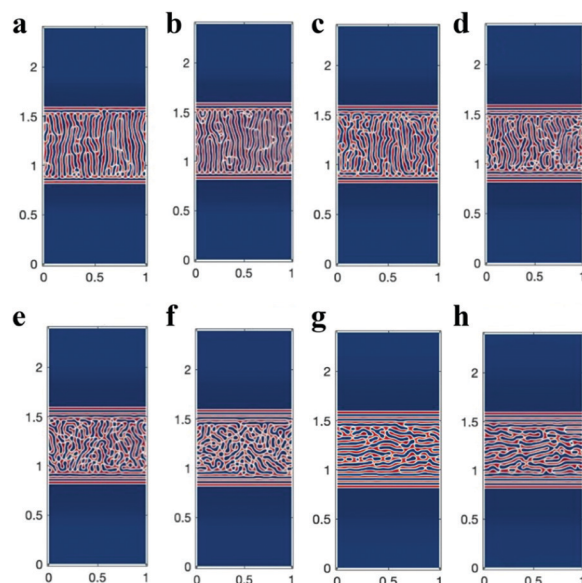
anisotropic mobility of the solvent does not generate the strip pattern if the polymer mobility is isotropic, as shown in Fig. 6b.

Fig. 7 displays the simulations with anisotropic polymer mobility.  $M_{px}$  is kept the same at 2.0.  $M_{py}$  increases gradually so that  $\theta$  decreases from a larger than unit value to a smaller than unit value. Near the boundary between the initial polymer–solution region and the coagulation bath, the polymer forms long strips parallel to the boundary at the end of simulation. However, within the initial polymer–solution region, the morphology exhibits a strong dependence on  $\theta$ . For  $\theta > 1$ , strip structures are parallel to the  $y$  axis. While for  $\theta < 1$ , they are along the  $x$  axis. That is, the strips prefer to align with the axis with a smaller mobility.

To demonstrate the sensitivity of porosity morphology to the anisotropy of polymer mobility further, and also to mimic a more realistic HFM dry-jet wet spinning process in the experiment,<sup>7</sup> we conduct simulations in 2D cylindrical coordinates for a sector area with  $0 < \theta < \pi/6$  as shown in Fig. 8. Initially, the polymer solution locates in the ring with  $r_i < r < r_o$ , and the regions with  $r < r_i$  and  $r > r_o$  contain the non-solvent phase. Periodic boundary conditions are applied in the azimuthal direction, while impermeable conditions are used in the inner and outer boundaries along the radial direction. We exclude the area  $r < r_c$  near the center to avoid the special treatment of the axis in the cylindrical coordinates. Since the polymer diffuses very slowly, for the current initial configuration, the polymer component does not reach the inner boundary at  $r_c$ . Meanwhile, the solvent diffuses much faster than the polymer. For a small  $r_c$  the solvent within the excluded region  $r < r_c$  should reach a uniform value close to the value



**Fig. 6** Membrane morphology of the water(n)/DMF(s)/PVDF(p) ternary system after phase separation shown by the contours of  $\phi_p$ . The red color represents the polymer-rich region. The initial polymer solution composite is  $(\phi_p, \phi_s) = (0.30, 0.65)$ . (a)  $(M_{sx}, M_{sy}) = (2000, 1000)$  and  $(M_{px}, M_{py}) = (2, 1)$ ; (b)  $(M_{sx}, M_{sy}) = (2000, 1000)$  and  $(M_{px}, M_{py}) = (2, 2)$ ; (c)  $(M_{sx}, M_{sy}) = (2000, 2000)$  and  $(M_{px}, M_{py}) = (2, 1)$ .



**Fig. 7** Membrane morphology with anisotropic polymer mobility of the water(n)/DMF(s)/PVDF(p) ternary system after phase separation shown by the contours of  $\phi_p$ . The red color represents the polymer-rich region. The initial polymer solution composite is  $(\phi_p, \phi_s) = (0.30, 0.65)$ .  $M_{px}$  is fixed at 2.0. From a to h,  $M_{py}$  is equal to 1.0, 1.2, 1.4, 1.6, 1.8, 2.0, 2.4, and 2.8, respectively.

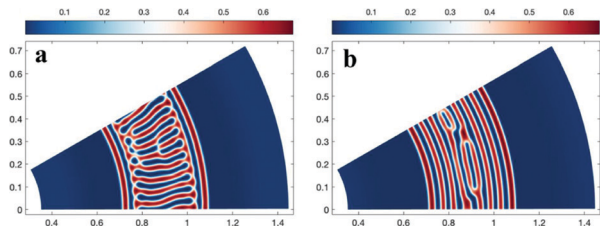


Fig. 8 Membrane morphology with tensor polymer mobility of the water(n)/DMF(s)/PVDF(p) ternary system in cylindrical coordinates after phase separation shown by the contours of  $\phi_p$ . The red color represents the polymer-rich region. The initial polymer solution composite is  $(\phi_p, \phi_s) = (0.30, 0.65)$ . (a)  $(M_{p\theta}, M_{p\phi}) = (2.0, 4.0)$  and (b)  $(M_{p\theta}, M_{p\phi}) = (4.0, 2.0)$ .

adjacent to the inner boundary. Therefore, the impermeable condition at the inner boundary is a reasonable approximation.

Anisotropy in the polymer mobility is introduced by setting  $M_{p\theta} \neq M_{p\phi}$ , and the anisotropy ratio is then calculated as  $\Theta = M_{p\theta}/M_{p\phi}$ . Fig. 8a and b show the polymer phase for  $\Theta = 2$  and  $0.5$ , respectively. Again, the strip-like patterns are formed with anisotropic polymer mobility, and the strips are along the directions with smaller polymer mobility. It is worth noting that the curvature of the boundary between the polymer solution and the coagulation bath does not change the overall behaviour of the porosity, as can be seen from the similarity between the simulations in the Cartesian box in Fig. 7 and those in cylindrical coordinates in Fig. 8.

## 4 Summary and conclusion

In summary, we investigate the Cahn–Hilliard phase field equation and its applications for the phase separation simulations of a ternary system. In particular, we introduce anisotropy into the polymer mobility, and focus on its influences on the porosity morphology of the formed polymer patterns. The anisotropy is implemented in the governing equation by a simple but heuristic method, which is, the mobility takes different values for the diffusion along two orthogonal axes. The model is tested for several two-dimensional configurations.

By the simulations of a fully periodic box, we systematically change the ratio of mobilities of two directions, and examine the obtained polymer patterns. The results reveal that as the ratio increases from unity which corresponds to the isotropic mobility, the porosity morphology quickly shifts to a strip dominant pattern and the strips orient along the direction with a smaller mobility. The influence of anisotropy saturates soon as the ratio further increases, and the strip pattern does not alter anymore.

The model with anisotropic mobility is then tested for a configuration which mimics the preparation of hollow fiber membranes. In this configuration the polymer solution is initially confined within a band or a circular ring of a finite width, with coagulation baths on both sides. For both a straight band or a circular ring, the anisotropic mobility can effectively produce strip patterns within the initial polymer solution region.

Our model of anisotropic mobility provides some interesting insights into rich polymer patterns produced by the phase separation of the ternary system. Since a polymer usually contains large molecules, diffusion with different rates along different directions seems to be a natural idea. Our results could be a possible mechanism for the various patterns in experiments. Also, by intentionally introducing anisotropy into the mobility, the resulting patterns may be controlled to certain extent. A more sophisticated model of anisotropic mobility can be developed in future work. One reasonable strategy is assuming that mobility takes different values along different directions with respect to the polymer concentration gradient.

## Conflicts of interest

There are no conflicts of interest to declare.

## Appendix

### Linear stability analysis

In this appendix we provide linear stability analysis for the model equations with anisotropic mobility coefficients for a homogeneous initial field. This method is similar to that in ref. 36. In accordance with our initial conditions, suppose a small perturbation is put over a homogeneous field of  $\phi_i$ 's, namely:

$$\phi_p(x, y, t) = \phi_p^0 + \varepsilon_p(t)e^{ik_x x + ik_y y}, \quad (\text{A.1})$$

$$\phi_s(x, y, t) = \phi_s^0 + \varepsilon_s(t)e^{ik_x x + ik_y y}, \quad (\text{A.2})$$

where  $\phi_p^0$  and  $\phi_s^0$  denote  $\phi_p$  and  $\phi_s$  at  $t = 0$ , respectively. We also assume  $|\varepsilon_p(t)| \ll 1$  and  $|\varepsilon_s(t)| \ll 1$ , at least initially. By substituting the above relationships into eqn (7) and (8) and taking the leading order term, we have:

$$\frac{d\varepsilon_p}{dt} = -M_{p\phi}(\Theta k_x^2 + k_y^2) \left[ (H_{pp}^0 \varepsilon_p + H_{ps}^0 \varepsilon_s) - K_p k^2 \varepsilon_p \right], \quad (\text{A.3})$$

$$\frac{d\varepsilon_s}{dt} = -M_s k^2 \left[ (H_{ps}^0 \varepsilon_p + H_{ss}^0 \varepsilon_s) - K_s k^2 \varepsilon_s \right], \quad (\text{A.4})$$

where  $k^2 = k_x^2 + k_y^2$  and  $H_{ij}^0 = \partial^2 f_0 / (\partial \phi_i \partial \phi_j)$ ,  $i, j = p, s$  denotes the Hessian of the bulk free energy  $f_0$  at  $t = 0$ . The above equations can be reorganized into the following vector form:

$$\frac{d\vec{\varepsilon}}{dt} = -\mathbf{M}\mathbf{H}^0\vec{\varepsilon} + k^2\mathbf{M}\mathbf{K}\vec{\varepsilon}, \quad (\text{A.5})$$

where  $\vec{\varepsilon} = (\varepsilon_p, \varepsilon_s)^T$ ,  $\mathbf{M} = \begin{bmatrix} M_{p\phi}(\Theta k_x^2 + k_y^2) & 0 \\ 0 & M_s k^2 \end{bmatrix}$ ,  $\mathbf{K} = \begin{bmatrix} K_p & 0 \\ 0 & K_s \end{bmatrix}$  and  $H^0$  denotes the matrix form of the Hessian and by combining eqn (1) and (5) we know that:

$$\frac{H^0}{RT} = \begin{bmatrix} (m_p \phi_p^0)^{-1} + (\phi_n^0)^{-1} - 2\chi_{np} & \chi_{sp} - \chi_{ns} - \chi_{np} + (\phi_n^0)^{-1} \\ \chi_{sp} - \chi_{ns} - \chi_{np} + (\phi_n^0)^{-1} & (\phi_s^0)^{-1} + (\phi_n^0)^{-1} - 2\chi_{ns} \end{bmatrix}. \quad (\text{A.6})$$

To observe interesting behaviour, *i.e.*, initially small perturbation  $\vec{\varepsilon}(t)$  to grow over time, a necessary condition is that  $H^0$  has at least one negative eigenvalue. It can be readily shown that

the above Hessian has a negative determinant given the initial conditions that we suggested in Section 3.1.

## Acknowledgements

JY acknowledges the partial support from the National Natural Science Foundation of China under Grant No. 52075482.

## References

- 1 M. Ulbricht, *Polymer*, 2006, **47**, 2217–2262.
- 2 H. Lonsdale, *J. Membr. Sci.*, 1982, **10**, 81–181.
- 3 M. Hashemi, S. Achenbach, D. Klymyshyn, B. Moazed and J. Lee, *Microsyst. Technol.*, 2010, **16**, 1563–1567.
- 4 J. Yin, PhD thesis, Clemson University, 2011.
- 5 B. Seifert, G. Mihanetzis, T. Groth, W. Albrecht and G. V. Sengbusch, *Artif. Organs*, 2002, **26**, 189–199.
- 6 X. Wang, X. Wang, L. Zhang, Q. An and H. Chen, *J. Macromol. Sci., Part B*, 2009, **48**, 696–709.
- 7 Z. Wang, J. Lin, D. Zhang, B. Xun, J. Yin, J. Qian, G. Dai, N. Zhang, X. Wen and Y. Huang, *J. Membr. Sci.*, 2019, 180–189.
- 8 G. T. Caneba and D. S. Soong, *Macromolecules*, 1985, **18**, 2538–2545.
- 9 Q. F. Alsally, *Sep. Sci. Technol.*, 2012, **48**, 234–245.
- 10 Y. Tang, N. Li, A. Liu, S. Ding, C. Yi and H. Liu, *Desalination*, 2012, **287**, 326–339.
- 11 J. J. Qin and T. Chung, *J. Membr. Sci.*, 1999, **157**, 35–51.
- 12 A. Ismail, M. Mustaffar, R. Illias and M. Abdullah, *Sep. Purif. Technol.*, 2006, **49**, 10–19.
- 13 P. Zhang, Y. Wang, Z. Xu and H. Yang, *Desalination*, 2011, **278**, 186–193.
- 14 D. Wang, K. Li and W. Teo, *J. Membr. Sci.*, 2000, **178**, 13–23.
- 15 X. Shen, Y. Zhao, Q. Zhang and L. Chen, *J. Polym. Res.*, 2013, **20**, 136.
- 16 M. Khayet, *Chem. Eng. Sci.*, 2003, **58**, 3091–3104.
- 17 E. P. Favvas, S. K. Papageorgiou, J. W. Nolan, K. L. Stefanopoulos and A. C. Mitropoulos, *J. Appl. Polym. Sci.*, 2013, **130**, 4490–4499.
- 18 B. Zhou and A. C. Powell, *J. Membr. Sci.*, 2006, **268**, 150–164.
- 19 H. H. Manuel and N. Ulrich, *J. Membr. Sci.*, 2018, **564**, 820–831.
- 20 D. R. Tree, K. T. Delaney, H. D. Cenicerros, T. Iwama and G. H. Fredrickson, *Soft Matter*, 2017, **13**, 3013–3030.
- 21 G. T. Caneba and D. S. Soong, *Macromolecules*, 1985, **18**, 2545–2555.
- 22 J. W. Cahn, *J. Chem. Phys.*, 1965, **42**, 93–99.
- 23 L.-P. Cheng, D.-J. Lin, C.-H. Shih, A.-H. Dwan and C. C. Gryte, *J. Polym. Sci. B: Polym. Phys.*, 1999, **37**, 2079–2092.
- 24 X. He, C. Chen, Z. Jiang and Y. Su, *J. Membr. Sci.*, 2011, **371**, 108–116.
- 25 A. Akthakul, C. E. Scott, A. M. Mayes and A. J. Wagner, *J. Membr. Sci.*, 2005, **249**, 213–226.
- 26 J. W. Cahn and J. E. Hilliard, *J. Chem. Phys.*, 1958, **28**, 258–267.
- 27 W. J. Boettinger, J. A. Warren, C. Beckermann and A. Karma, *Annu. Rev. Mater. Res.*, 2002, **32**, 163–194.
- 28 R. Folch, J. Casademunt, A. Hernández-Machado and L. Ramírez-Piscina, *Phys. Rev. E*, 1999, **60**, 1734–1740.
- 29 S. Yook, T. Isik, V. Ortalan and M. Cakmak, *Soft Matter*, 2020, **16**, 2104–2113.
- 30 T. A. Hunt and B. D. Todd, *J. Chem. Phys.*, 2009, **131**, 054904.
- 31 H. D. Vuijk, J. M. Brader and A. Sharma, *Soft Matter*, 2019, **15**, 1319–1326.
- 32 R. Verzicco and P. Orlandi, *J. Comput. Phys.*, 1996, **123**, 402–414.
- 33 M. M. Rai and P. Moin, *J. Comput. Phys.*, 1991, **96**, 15–53.
- 34 S. Feng, X. Xiong, G. Zhang, N. Xia, Y. Chen and W. Wang, *Macromolecules*, 2009, **42**, 281–287.
- 35 Y. Nie, G. Huang, L. Qu, X. Wang, G. Weng and J. Wu, *Polymer*, 2011, **52**, 3234–3242.
- 36 J. F. Blowey, M. I. M. Copetti and C. M. Elliott, *IMA J. Numer. Anal.*, 1996, **16**, 111–139.